


Cite this: *Chem. Sci.*, 2020, **11**, 11042

All publication charges for this article have been paid for by the Royal Society of Chemistry

# Regiocontrol in the oxidative Heck reaction of indole by ligand-enabled switch of the regioselectivity-determining step†

Yu-Jie Wang, Chen-Hui Yuan, De-Zhao Chu and Lei Jiao \*

Efficient control of regioselectivity is a key concern in transition-metal-catalyzed direct C–H functionalization reactions. Various strategies for regiocontrol have been established by tuning the selectivity of the C–H activation step as a common mode. Herein, we present our study on an alternative mode of regiocontrol, in which the selectivity of the C–H activation step is no longer a key concern. We found that, in a reaction where the C–H activation step exhibits a different regio-preference from the subsequent functionalization step, a ligand-enabled switch of the regioselectivity-determining step could provide efficient regiocontrol. This mode has been exemplified by the Pd(II)-catalyzed aerobic oxidative Heck reaction of indoles, in which a ligand-controlled C3-/C2-selectivity was achieved for the first time by the development of sulfoxide-2-hydroxypyridine (SOHP) ligands.

Received 21st April 2020  
Accepted 13th September 2020

DOI: 10.1039/d0sc02246b

rsc.li/chemical-science

## 1. Introduction

Control of regioselectivity is a key concern in organic synthesis when the substrate bears more than one potential reactive site. The transition-metal-catalyzed C–H functionalization reactions represent an appealing approach to molecular modification,<sup>1</sup> in which the substrates always contain more than one reactive C–H bonds, and efficient regiocontrol is of great significance. A variety of classical strategies have been developed to achieve this goal, generally focusing on the C–H activation step (Scheme 1a). For instance, in the C–H functionalization reactions of (hetero)arenes, a directing group (DG) strategy (for *ortho*-functionalization)<sup>2</sup> and a template strategy (for remote functionalization)<sup>3</sup> have been widely used for regiocontrol. For arenes without a suitable DG, many C–H functionalization reactions were reported to occur at the site prone to C–H activation (referred to as intrinsic regiocontrol).<sup>4</sup>

Catalyst control is another useful strategy for tuning the regioselectivity. In particular, ligand development in the transition-metal-catalyzed C–H functionalization reactions has attracted significant attention in recent years,<sup>5–7</sup> and ligand-enabled regiocontrol has emerged as a promising strategy. Representative advances in this direction arose from the field of Pd(II) catalysis,<sup>6</sup> in which a few examples have been reported to achieve ligand-dictated regioselectivity in the C–H functionalization of arenes: Itami and co-workers reported ligand-

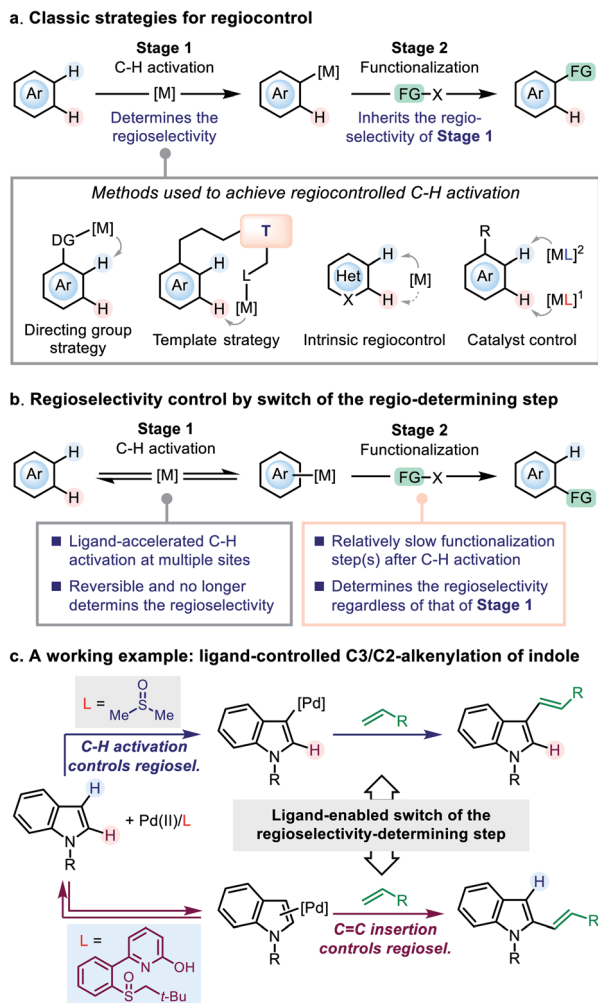
controlled  $\alpha$ -/ $\beta$ -arylation of thiophenes;<sup>8</sup> the Yu group achieved regioselectivity control in the C–H alkenylation of arenes by using mono-protected amino acid (MPAA) ligands;<sup>6a</sup> the Stahl group utilized 4,5-diazafluorene (DAF) ligands to switch the C3-/C2-selectivity in the arylation of indole;<sup>6a</sup> the Sanford group demonstrated the role of pyridine as a ligand to dictate the regioselectivity of chloroarene acetoxylation;<sup>6k</sup> Carrow and co-workers developed a thioether-based ligand to tune the regioselectivity of the thiophene alkenylation.<sup>6v</sup> These studies highlighted the concept of ligand control in the C–H activation step; however, to date the principle of ligand design toward a desired regioselectivity on a given substrate remains ambiguous.

Herein, we present our study on an alternative mode of ligand-dictated regiocontrol, in which the selectivity of the C–H activation step is no longer a key concern (Scheme 1b). We envisioned that, when the functionalization step exhibits a different regio-preference from the C–H activation step, regiocontrol could be achieved by simply switching the regioselectivity-determining step of the reaction (*i.e.*, the switch from scenario a to b described in Scheme 1), and suitably designed ancillary ligands could do this job by accelerating C–H metalation at multiple sites to make the C–H activation step reversible and no longer regioselectivity-determining. Although the principle is simple, such an example was rare in the literature and the development of such ligands remained challenging.<sup>9</sup>

In the present work, we take the Pd(II)-catalyzed oxidative C–H alkenylation reaction of indole derivatives as a working example to demonstrate this mode of regiocontrol (Scheme 1c). Owing to the development of a novel sulfoxide-2-hydroxypyridine (SOHP) ligand, the ligand-controlled C3-/C2-

Center of Basic Molecular Science (CBMS), Department of Chemistry, Tsinghua University, Beijing 10084, China. E-mail: lejiao@mail.tsinghua.edu.cn

† Electronic supplementary information (ESI) available. CCDC 1978349 and 1978351. For ESI and crystallographic data in CIF or other electronic format see DOI: 10.1039/d0sc02246b



Scheme 1 Regiocontrol in transition-metal-catalyzed C–H functionalization.

selectivity in this reaction was achieved for the first time by the switch of the regioselectivity-determining step. The in-depth mechanistic study has disclosed a clear picture of this control mode, which may provide inspirational insights into the ligand design and regiocontrol in related catalytic systems.

## 2. Results and discussion

The indole motif is the key substructure of many natural products, pharmacophores, and synthetic building blocks, and the methods for regioselective direct C–H functionalization of indole are highly demanded. Indole has long been employed as a typical substrate in various Pd(II)-catalyzed C–H functionalization reactions,<sup>10,11</sup> and among them the oxidative C–H alkenylation (the oxidative Mizoroki–Heck reaction)<sup>12</sup> of indole was selected as a suitable model reaction for the present study, because it has a well-established mechanistic picture, while the ligand-enabled regioselectivity control is unprecedented to date.

It was established that the Pd(II)-catalyzed C–H alkenylation of indole took place at the C3-position with a high

regioselectivity, which was attributed to a regioselectivity-determining C–H palladation step that preferentially occurs at the C3-position.<sup>13</sup> The intrinsic C3-selectivity makes the selective C2-alkenylation of indole a difficult yet highly demanding task. While a number of protocols have been developed to achieve N1-, C2-, or C3-selective C–H arylation reaction of indole,<sup>10c,14</sup> there are only a few methods to switch the site-selectivity of indole alkenylation from C3 to C2, such as the DG strategy<sup>15</sup> or a solvent- or oxidant-controlled regioselectivity.<sup>13e,16</sup> A ligand-enabled regiocontrol has not been worked out for this reaction. Aiming at developing a suitable catalytic system that allows for a ligand-controlled C3-/C2-alkenylation reaction of indole, we set out to investigate the origin of the intrinsic C3-alkenylation selectivity in the model reaction.

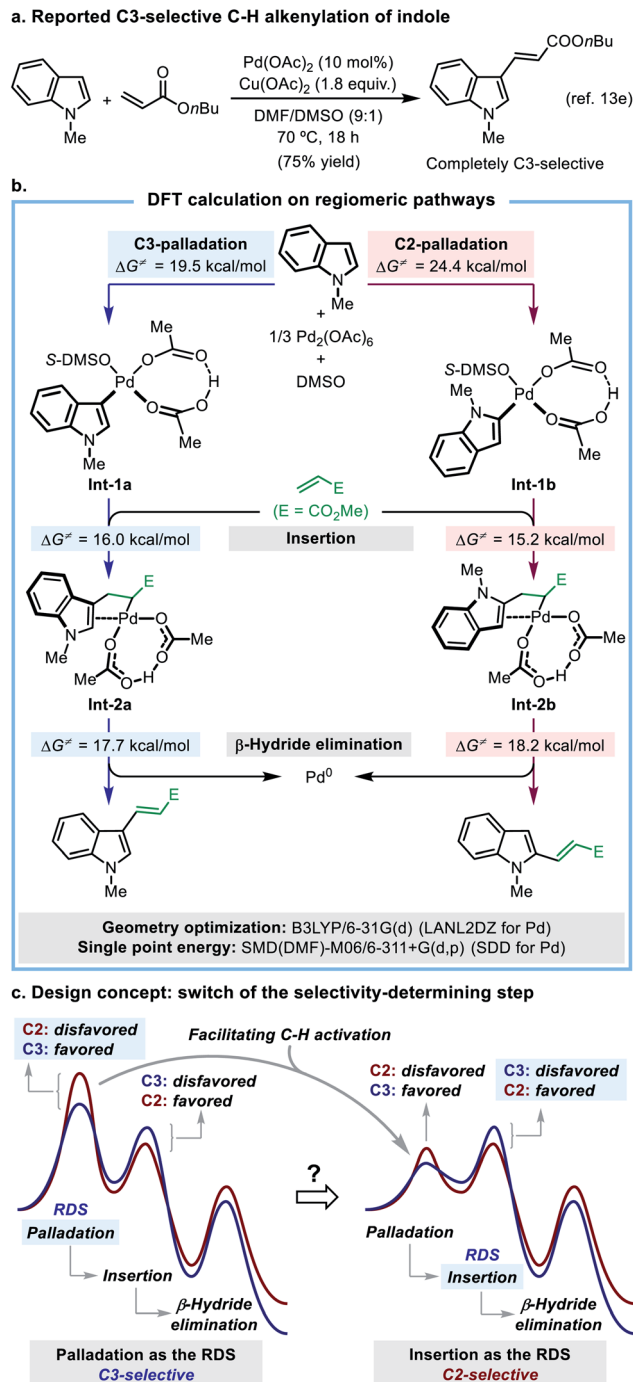
### 2.1 Understanding the intrinsic regioselectivity of the oxidative Heck reaction of indole

**DFT computational study.** First, the reaction between *N*-methylindole and methyl acrylate catalyzed by Pd(OAc)<sub>2</sub> under the established “ligandless” conditions<sup>13e</sup> was modeled by DFT calculation (Scheme 2a).<sup>17</sup> While the DFT study on the same reaction has been reported,<sup>18</sup> only the C3-alkenylation pathway was calculated and no attention was paid to the origin of regioselectivity. In this study, we performed the calculation with a particular focus on the regiomer pathways leading to both C3- and C2-products (Scheme 2b).

In this mechanistic scheme, each regiomer pathway is composed of three crucial steps including palladation, insertion, and  $\beta$ -hydride elimination (for full potential energy surfaces, see Fig. S12<sup>†</sup>). Palladation is an irreversible rate-determining step (RDS) in both pathways, which determines the overall regioselectivity of the reaction. The C3-palladation has a lower activation energy barrier (19.5 kcal mol<sup>−1</sup>) than that of the C2-palladation (24.4 kcal mol<sup>−1</sup>), which well accounts for the observed C3-selectivity. A simplified potential energy surface (Scheme 2c, left side) clearly illustrates the mode of regioselectivity control in this reaction. The key finding of the DFT study is that the C=C insertion step after palladation exhibits a reversed regio-preference, with the C2-insertion ( $\Delta G^\ddagger = 15.2$  kcal mol<sup>−1</sup>) being kinetically more favorable than the C3-insertion ( $\Delta G^\ddagger = 16.0$  kcal mol<sup>−1</sup>). This is an important piece of mechanistic information that has not been disclosed in previous studies.

**Potential solution for tuning the regioselectivity.** Based on the above mechanistic understanding, we planned to achieve the regiocontrol of this reaction by taking advantage of the reversed regio-preference of the alkene insertion step. Encouraged by the pioneering studies on the ligand effect on transition-metal-catalyzed C–H activation reactions, we envisioned that, by introducing a suitably designed ancillary ligand that could remarkably accelerate C–H metalation, the palladation step might become reversible and the following insertion step could be made regioselectivity-determining (Scheme 2c, right side). In this scenario, the selectivity of the palladation step is no longer decisive, and the selectivity-determining insertion step might render an overall C2-selectivity. This





Scheme 2 Understanding the origin of regioselectivity in the model reaction.

strategy is referred to as a ligand-enabled switch of the regioselectivity-determining step.

## 2.2 Ligand design and preliminary studies

**Design concept.** Based on the aforementioned idea, we set out to consider a blueprint for ligand design (Fig. 1). Given that the ligand should facilitate C–H metalation to make both C3- and C2-palladation of indole kinetically accessible, it was clear that the key element of the ligand should be a basic group (B),

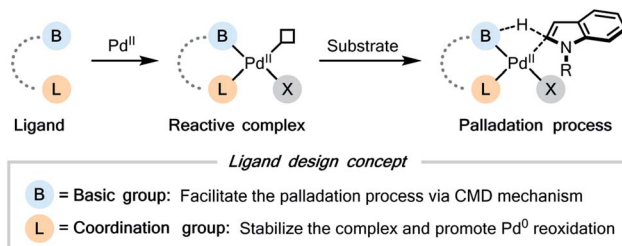


Fig. 1 Ligand design.

which acts as an internal base to promote C–H palladation *via* a concerted metalation–deprotonation (CMD) mechanism. In addition, we thought that a suitable coordination group (L) might be beneficial, as an additional coordination site could stabilize the Pd(II)–ligand complex and facilitate the re-oxidation of Pd(0).

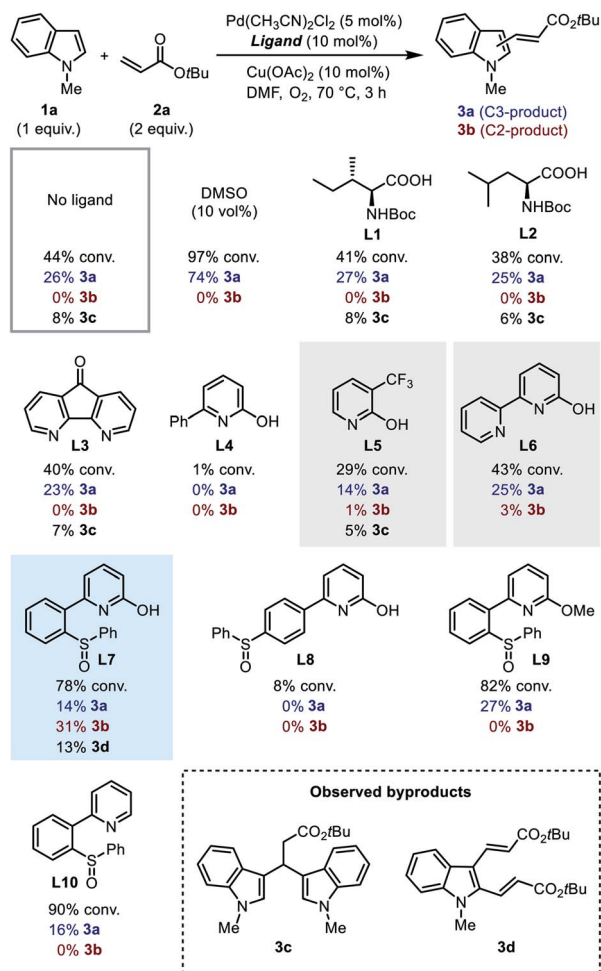
Then we further considered the detailed structure of the possible ligands. Both the acylamide (RCONH) group<sup>6c–g</sup> and the 2-hydroxypyridine (2-pyridone) group<sup>19</sup> were known as efficient proton shuttle in the previous ligand design, thus we chose them as the potential basic group of the ligand. For the coordination group, a nitrogen- or oxygen-centered coordination site, such as pyridine, oxazoline, and carboxylic acid, was a typical choice. For the tether connecting two subunits of the ligand, either an alkyl chain or an aryl ring might be suitable.

We first searched in the established library of ligands that have been demonstrated to be efficient in Pd(II)-catalyzed C–H functionalization reactions. Among them, MPAAAs match the above design, thus Boc-Ile-OH (**L1**) and Boc-Leu-OH (**L2**) were picked out as the representative members. DAF ligand **L3**, which was proved effective in promoting the C2-selective arylation of indole,<sup>6a</sup> was also selected. 6-Phenyl-2-pyridinol (**L4**) and 3-trifluoromethyl-2-pyridinol (**L5**)<sup>20</sup> were chosen to evaluate the effect of the 2-hydroxypyridine motif alone. Finally, we added [2,2'-bipyridin]-6(1*H*)-one (bipy-6-OH, **L6**), a ligand that was reported to remarkably accelerate the CMD process in palladium catalysis.<sup>21</sup> We intended to test the performance of these candidate ligands in the model oxidative Heck reaction of indole, with the hope that some of them could exhibit the desired C2-selectivity.

**Preliminary ligand test.** The effect of ligands was evaluated by comparing the results from a model reaction performed with and without a ligand (Scheme 3). Based on the previous reports on the oxidative Heck reaction of indole, we developed a set of reaction conditions that allow for efficient aerobic oxidative coupling between *N*-methylindole (**1a**) and *tert*-butyl acrylate (**2a**) as the platform for ligand evaluation. We employed 5 mol% PdCl<sub>2</sub>(CH<sub>3</sub>CN)<sub>2</sub> as the Pd(II) source, 10 mol% Cu(OAc)<sub>2</sub> as the redox catalyst to promote Pd(0) reoxidation, and *N,N*-dimethylformamide (DMF) as the solvent. The reaction was performed under 1 atm of O<sub>2</sub> at 70 °C. This set of conditions avoided the use of a stoichiometric amount of Cu(II) salt, which made the reaction solution homogeneous and minimized undesired ligand complexation to copper.

It was found that without a ligand the model reaction reached a moderate conversion to afford a low yield of C3-





Scheme 3 Ligand effects on the model reaction. Conversions were determined by GC analysis, and yields were determined by <sup>1</sup>H NMR analysis.

alkenylation product **3a**, and palladium black formation was observed. With the addition of 10 vol% dimethylsulfoxide (DMSO) as a supporting ligand to prevent the aggregation of Pd(0), both the conversion of **1a** and the yield of **3a** increased dramatically, and the reaction remained completely C3-selective. To our disappointment, MPAA ligands **L1** and **L2** did not show an obvious promotive effect compared with the ligand-free conditions, nor did they alter the regioselectivity. In these reactions a minor amount of byproduct **3c** resulting from Michael addition of indole to the C3-product **3a** was obtained. DAF ligand **L3** produced a similar result. For 2-hydroxypyridine-based ligands, ligand **L4** had an inhibitory effect on the reaction, and both ligands **L5** and **L6** exhibited a low C3-reactivity. Interestingly, in the reactions with ligands **L5** and **L6**, a trace amount of the C2-product was observed in the crude <sup>1</sup>H NMR (<3%), which was never observed with other ligands. This observation indicated that the 2-hydroxypyridone motif might indeed be a key element in the ligand. Despite this, in general the established ligand library is not competent for regioselective C2-alkenylation of indole, which demonstrated the challenge for ligand design.

**Development of the SOHP ligands.** Next we conceived a new ligand design employing the 2-hydroxypyridine motif as the basic group. We noticed that, DMSO was recognized as an efficient supporting ligand in many Pd(II)-catalyzed C–H functionalization reactions, and sulfoxide is an emerging substructure in the ligands for Pd(II).<sup>22</sup> Therefore, we decided to employ a phenyl sulfoxide moiety as the coordination group. A benzene ring was chosen as the backbone, and the resulting ligand was named sulfoxide-2-hydroxypyridine (SOHP). To our delight, this newly designed ligand **L7** increased the C2-selectivity dramatically, favouring the C2-product over the C3-product (Scheme 3). In addition, the 2,3-bisalkenylation byproduct **3d** was produced in a minor amount, which was also attributed to the C2-alkenylation.

In order to probe the role of the two subunits in the SOHP ligand, partially modified ligands **L8–L10** were tested (Scheme 3). When the sulfoxide moiety was moved from the *ortho*- to the *para*-position (**L8**), the catalytic activity lost completely, which supports the role of the sulfoxide as a coordination group rather than merely an electronic substituent. Blocking of the hydroxyl group by a methyl group (**L9**) or removal of the hydroxyl group (**L10**) in the ligand led to loss of C2-selectivity while maintaining a diminished reactivity. These results emphasized the important role of both 2-hydroxypyridine and sulfoxide subunits in dictating the C2-selectivity, as well as the cooperative effect of these two subunits.

**Optimization of the ligand structure.** We further studied the structure–activity relationship of the SOHP ligand (Table 1). The reactions were carried out employing Cu(OTf)<sub>2</sub> as the copper source instead of Cu(OAc)<sub>2</sub>, since it improved the activity of the catalytic system (entry 1). For the substitution on the sulfoxide motif, the electron-deficient aryl group was inferior to electron-rich ones (entries 1–3). An alkyl group in place of an aryl group in the sulfoxide moiety generally improved the C2-selectivity, and bulkier alkyl groups exhibited improved activity (entries 4–9). A sulfoxide-2-hydroxyquinoline (SOHQ) ligand **L19** could also promote C2-alkenylation with good regioselectivity, albeit the activity was not satisfactory (entry 10). A methylene-tethered SOHP ligand **L20** showed similar activity and regioselectivity to its benzene-tethered counterpart **L7** (entry 11). Interestingly, it was found that the presence of DMSO (10 vol%) interfered with the SOHP ligand-promoted reaction, leading to both low yield and low C2-selectivity of the alkenylation product (entry 12). Finally, with the optimal ligand **L17**, we found that the use of Cu<sub>2</sub>(OH)<sub>2</sub>CO<sub>3</sub> as the redox catalyst and a 2 : 1 ratio of indole to acrylate were suitable reaction conditions for the desired C2-alkenylation (entries 13–16).

At this stage, we had identified a new ligand design that enables the unusual C2-selectivity in the oxidative Heck reaction of indole based on the concept of ligand-controlled switch of the rate-determining step. Our next goal was to draw a clear mechanistic picture of this control mode by a detailed mechanistic study.

### 2.3 Mechanistic studies

**Structure of the Pd(II)–SOHP complex.** We studied the structure of the Pd(II)–SOHP complex by independent



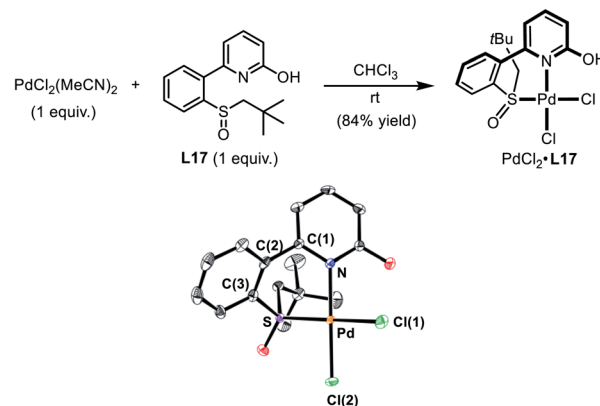
Table 1 Ligand optimization<sup>a</sup>

Entry	Ligand	Conv.	3a	3b	3d	Overall
1	L7	86%	12%	41%	10%	63%
2	L11	42%	—	9%	—	9%
3	L12	81%	10%	42%	10%	62%
4	L13	23%	1%	13%	—	14%
5	L14	34%	4%	24%	—	28%
6	L15	43%	6%	26%	2%	34%
7	L16	59%	4%	34%	2%	40%
8	L17	83%	6%	46%	6%	58%
9	L18	65%	6%	40%	5%	51%
10	L19	36%	—	17%	—	17%
11	L20	82%	10%	37%	4%	51%
12 <sup>b</sup>	L17	53%	12%	14%	—	26%
13 <sup>c</sup>	L17	58%	10%	43%	4%	54%
14 <sup>c,d</sup>	L17	96%	6%	50%	15%	71%
15 <sup>c,d,e</sup>	L17	—	7%	46%	12%	65%
16 <sup>c,d,e,f</sup>	L17	—	5%	63%	8%	76%

<sup>a</sup> Conversions were determined by GC analysis, and yields were determined by <sup>1</sup>H NMR analysis. <sup>b</sup> 10 vol% of DMSO was added. <sup>c</sup> 50 mol% of Cu<sub>2</sub>(OH)<sub>2</sub>CO<sub>3</sub> was used instead of Cu(OTf)<sub>2</sub>. <sup>d</sup> 10 mol% PdCl<sub>2</sub>(CH<sub>3</sub>CN)<sub>2</sub> was employed. <sup>e</sup> 2 equiv. of **1a** and 1 equiv. of **2a** were used, and the yields were calculated based on the amount of acrylate. <sup>f</sup> Reaction was performed at 50 °C for 12 h.

preparation of the complex from PdCl<sub>2</sub>(CH<sub>3</sub>CN)<sub>2</sub> and **L17** in CHCl<sub>3</sub> (Scheme 4). A crystalline complex was obtained in a good yield, and the single crystal X-ray diffraction (XRD) analysis revealed that it was the expected Pd(II)–SOHP complex PdCl<sub>2</sub>·**L17**, in which the ligand adopts a κ<sup>2</sup>-N,S coordination mode. It is notable that the two aromatic rings are not co-planar, which have a torsion angle of *ca.* 45°. <sup>1</sup>H NMR analysis confirmed the homogeneity of the crystalline PdCl<sub>2</sub>·**L17** and the complex prepared *in situ* in DMF, and the complex PdCl<sub>2</sub>·**L17** exhibited similar activity and selectivity to that of the PdCl<sub>2</sub>(CH<sub>3</sub>CN)<sub>2</sub>/L17 system, implying that this complex might be a precatalyst in the catalytic cycle.

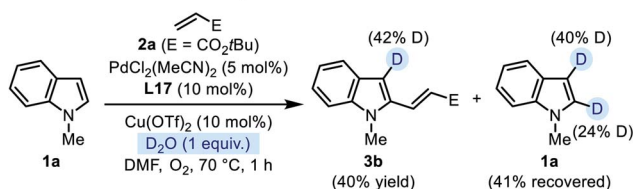
**Deuterium labeling experiments.** To investigate the regioselectivity and reversibility of the C–H palladation step under ligand control, we performed deuterium labeling experiments. First, the model reaction between **1a** and **2a** was done under the standard conditions (Table 1, entry 8) with the addition of 1 equiv. of D<sub>2</sub>O, and the reaction was interrupted at about half



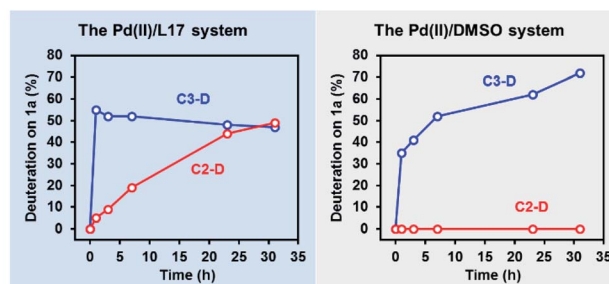
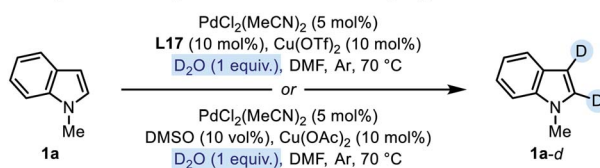
Scheme 4 Preparation of the Pd(II)–SOHP Complex. In the ORTEP plot of PdCl<sub>2</sub>·**L17** (CCDC 1978349), thermal ellipsoids are drawn at 50% probability level. The co-crystallized CHCl<sub>3</sub> and all H atoms are omitted for clarity. Selected distances (Å) and a dihedral angle (deg): Pd–N 2.079(3), Pd–S 2.226(1), Pd–Cl(1) 2.324(1), Pd–Cl(2) 2.277(1), and N–C(1)–C(2)–C(3) 44.9(5).

conversion. It was found that, there was significant deuterium incorporation at both C2- and C3-positions of the recovered *N*-methylindole and the C3-position of product **3b** (Scheme 5a). A control experiment has shown that in the absence of the SOHP ligand, the H/D exchange merely occurred at the C3-position, and the C2-position remained intact. Given that the H/D exchange at the C3-position of indole occurs facilely even in the absence of Pd(II),<sup>23</sup> this observation suggested that the C2-palladation is reversible in the catalytic cycle, which is only made possible by using the Pd(II)/L17 system.

#### a. Proof of a reversible C2-palladation



#### b. Independent study on the C–H deuteration progress



Scheme 5 Probing the C2-palladation by deuteration.

Then we performed an independent study on the deuteration of *N*-methylindole by running the reaction in the absence of **2a**. The progress of both C3- and C2-deuteration was monitored as an indicator of C–H palladation at the corresponding site. In the Pd(II)/**L17** system, the C3-deuteration occurred more rapidly than the C2-deuteration, but finally deuterium incorporation at both sites reached the same level (Scheme 5b, the left plot). In contrast, in the Pd(II)/DMSO system (the established C3-alkenylation conditions), only C3-deuteration was observed, which occurred slower than that in the Pd(II)/**L17** system (Scheme 5b, the right plot). The contrast made clear that, compared with the Pd(II)/DMSO system, the Pd(II)/**L17** system accelerates the C–H palladation process to make both C3- and C2-palladation kinetically accessible, while the regio-preference of the C–H activation step remains unchanged.

We noticed that the C2-deuteration of indole **1a** proceeded more rapidly in the ligand-promoted oxidative Heck reaction than in the independent deuterium labeling experiment with Pd(II)/**L17**. Although a rigorous rationalization of this phenomenon has not been worked out at present, we tentatively attributed this difference to the different basicity of the two reaction systems.<sup>24</sup> Nevertheless, the results from the deuterium labeling experiments revealed a reversible palladation at both C3- and C2-positions of indole enabled by the SOHP ligand, which confirmed our design concept that the ligand effect might render the C–H activation step reversible and no longer regioselectivity-determining.

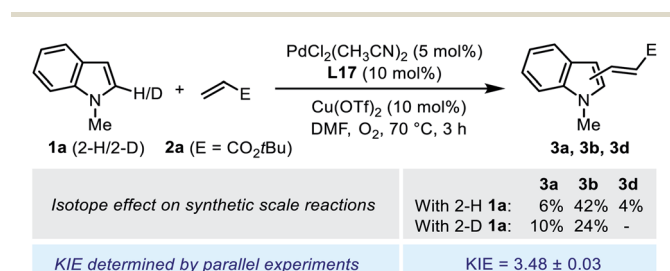
**Isotope effect.** Subsequently, we studied the isotope effect on the C2-alkenylation process of the model reaction. For a synthetic scale reaction employing C2-deuterated **1a**, the yield of the C2-alkenylation product **3b** was found to be remarkably lower than that in the standard reaction employing non-deuterated **1a**, leading to a diminished C2-selectivity (Scheme 6).

Parallel initial rate measurements were performed by employing 2-H and 2-D indole substrate **1a** to determine the apparent kinetic isotope effect (KIE) of the reaction. The determined KIE of *ca.* 3.5 was consistent with the observation in the synthetic scale reaction (Scheme 6), and these results indicated a significant primary KIE for the C–H cleavage step. Normally, such a remarkable isotope effect indicates a rate-limiting irreversible C–H activation. However, it seemed contradictory to the reversible nature of the C–H palladation step revealed by the deuterium labeling experiment (Scheme 5a). We reasoned that, in the Pd(II)/SOHP reaction system, the

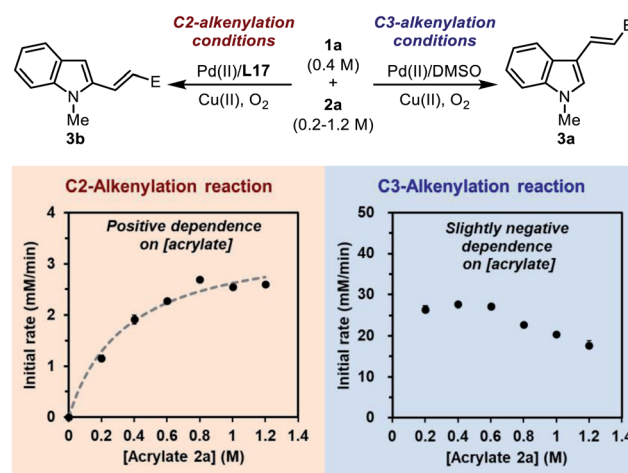
activation energy barriers of the C–H palladation step and its following step were comparable to each other, thus the reaction could exhibit both a reversible C–H activation step and a significant apparent primary KIE, and this could be referred to as a quasi-reversible C–H activation. Interestingly, a similar circumstance has also been observed in the Pd(II)-catalyzed alkenylation reaction of thiophene derivatives, where a significant primary KIE was observed while the C–H activation step remained reversible.<sup>25</sup> To figure out the rate-limiting step of the overall reaction, further experimental study was required.

**Probing the rate-limiting step.** We set out to figure out whether or not the C=C insertion step following C–H palladation is rate-limiting. The initial rate of the model reaction promoted by the Pd(II)/**L17** system was measured with different acrylate concentrations (Scheme 7, the left plot). It was found that the C2-alkenylation reaction exhibited a clear positive dependence on [acrylate] within the range of 0.2–1.2 M, which seemed to follow a saturation kinetics. This implied that the migratory C=C insertion step after C–H palladation played an important role in determining the rate of the reaction. Given the quasi-reversible C–H activation step revealed previously, we reasoned that this saturation-like kinetics did not imply a saturated pre-coordination equilibrium as usual, but instead reflected the result of the similar activation energy barriers of the C–H palladation step and the following insertion step. Taking these results together, it could be concluded that none of the two steps was a clear-cut rate-limiting step in the catalytic cycle, and both steps were important in determining the rate of the overall reaction.

For comparison, the dependence of the initial rate on [acrylate] in the C3-alkenylation reaction catalyzed by the Pd(II)/DMSO system was also studied (Scheme 7, the right plot). Interestingly, a distinct dependence profile over the same range of [acrylate] was obtained, in which the initial rate was zero-order at low [acrylate] and gradually exhibited a negative-order at high [acrylate]. This result was consistent with a rate-limiting C–H activation step in the normal C3-alkenylation reaction of indole revealed by the DFT calculation (Scheme



Scheme 6 Study of isotope effect on C2-alkenylation.



Scheme 7 Effect of acrylate loading on the reaction.





2b). The negative order observed at high [acrylate] might be attributed to the competitive coordination of the acrylate substrate to the catalytic center that led to off-cycle species.

The results shown above manifested a change of the reaction profile from an irreversible rate-limiting C–H palladation (in the Pd(II)/DMSO system) to a complex rate-determining scenario with a quasi-reversible C–H palladation (in the Pd(II)/SOHP system). This supported our proposal that the ligand effect was able to switch the mode of rate- and selectivity-control in the catalytic cycle. The reversibility of the C–H palladation step implied that the C=C migratory insertion step might play an important role in determining the regioselectivity, which was to be clarified by further studies.

**Regioselectivity of the insertion step.** Next, we attempted to use norbornene to trap the palladated indole species after the C–H activation step. Because the insertion product of norbornene could not undergo further  $\beta$ -hydride elimination due to the lack of a co-planar  $\beta$ -hydrogen, such an insertion intermediate might be isolated to gain some insight into the regio-preference of the insertion step.

To this end, two stoichiometric reactions between *N*-methylindole and norbornene were performed with both Pd(II)/DMSO (the C3-alkenylation conditions) and Pd(II)/L17 systems (the C2-alkenylation conditions). To our delight, the reaction could indeed stop after the insertion step, and upon treatment with NaBH<sub>4</sub>, the insertion intermediates afforded the corresponding norborylindole products (Scheme 8). It was found that, without the SOHP ligand, this reaction sequence only produced 3-norborylindole **5a**, supporting an exclusive C3-

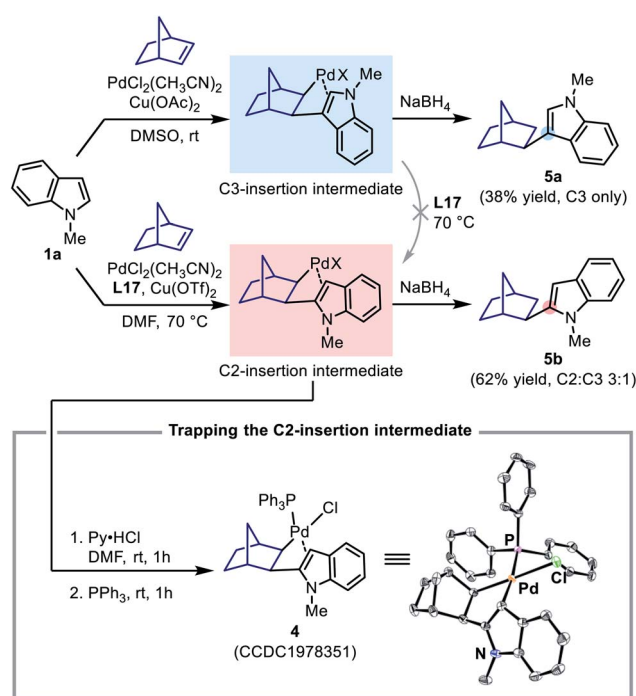
palladation/insertion. In contrast, with the SOHP ligand, 2-norborylindole **5b** was obtained as the major product together with a minor amount of **5a** (C2 : C3 = 3 : 1). Furthermore, if the crude C2-insertion intermediate formed in the Pd(II)/L17 system was treated with pyridinium hydrochloride (for anion exchange) and then triphenylphosphine (for coordination), the PPh<sub>3</sub>-coordinated C2-insertion complex **4** could be isolated in pure form by column chromatography, whose structure was confirmed by single crystal XRD analysis (Scheme 8).

The formation of the C2-insertion intermediate demonstrated the crucial role of the SOHP ligand in enabling the C2-palladation/C2-insertion pathway. However, because the insertion of norbornene into a C–Pd bond was found to be reversible in some cases, the formation of the C2-insertion intermediate could be rationalized either as a result of selective C2-insertion (kinetic control) or as an outcome of the equilibrium between insertion products (thermodynamic control). We found that, upon addition of stoichiometric ligand L17 to the generated C3-insertion intermediate and treatment at 70 °C, the C3-insertion intermediate remained intact and could not be transformed to its C2-counterpart, suggesting that the equilibrium between the regiomer insertion products in the presence of the SOHP ligand was not viable. Therefore, the above results with norbornene served as a direct evidence for the C2-insertion process promoted by the SOHP ligand, and corroborated a regioselectivity-determining insertion step in the catalytic cycle.

**DFT computational study.** At this stage, we approached a brief mechanistic picture of the C2-alkenylation of indole enabled by the SOHP ligand: (1) the Pd(II)–SOHP complex makes both C3- and C2-palladation of indole kinetically accessible and quasi-reversible, with the C3-palladation more favorable; (2) the mode of rate- and regioselectivity-control has been significantly changed by the involvement of the SOHP ligand, in which the C=C migratory insertion step played an important role; (3) the alkene insertion step exhibits a C2-selectivity and determines the overall regioselectivity.

In order to gain further details of the reaction mechanism, we performed a DFT computational study on the model reaction between **1a** and **2b** promoted by using the Pd(II)/SOHP ligand/Cu(OTf)<sub>2</sub> system (Fig. 2).<sup>17</sup> Methyl SOHP L13 was selected as a representative ligand for computational modeling to save computation time, because L13 exhibited similar C2-selectivity in the model reaction compared with the optimal ligand L17, though with an inferior reactivity.

The reaction starts from the Pd(II)–ligand complex PdCl<sub>2</sub>·L13. In order to accommodate the indole substrate, a chloride anion should leave the Pd(II) center to make a vacant coordination site. This could be achieved by elimination of HCl from the complex to form **Int-3**, which is highly endergonic ( $\Delta G > 20$  kcal mol<sup>−1</sup>) according to the computational result (see the ESI† for details). We found that, when the HCl elimination process is coupled with the trapping of protons by the free SOHP ligand and the coordination of Cl<sup>−</sup> to Cu(II), its thermodynamic barrier becomes reasonable ( $\Delta G = 7.6$  kcal mol<sup>−1</sup>). Although there might still be some error in the calculated free energy of the deprotonation step due to the complexity of the reaction system, it was clear that the acid–base interaction



**Scheme 8** Study on the regioselectivity of the alkene insertion step. In the ORTEP plot of **4**, thermal ellipsoids are drawn at the 50% probability level. The co-crystallized CH<sub>2</sub>Cl<sub>2</sub> and all H atoms are omitted for clarity.

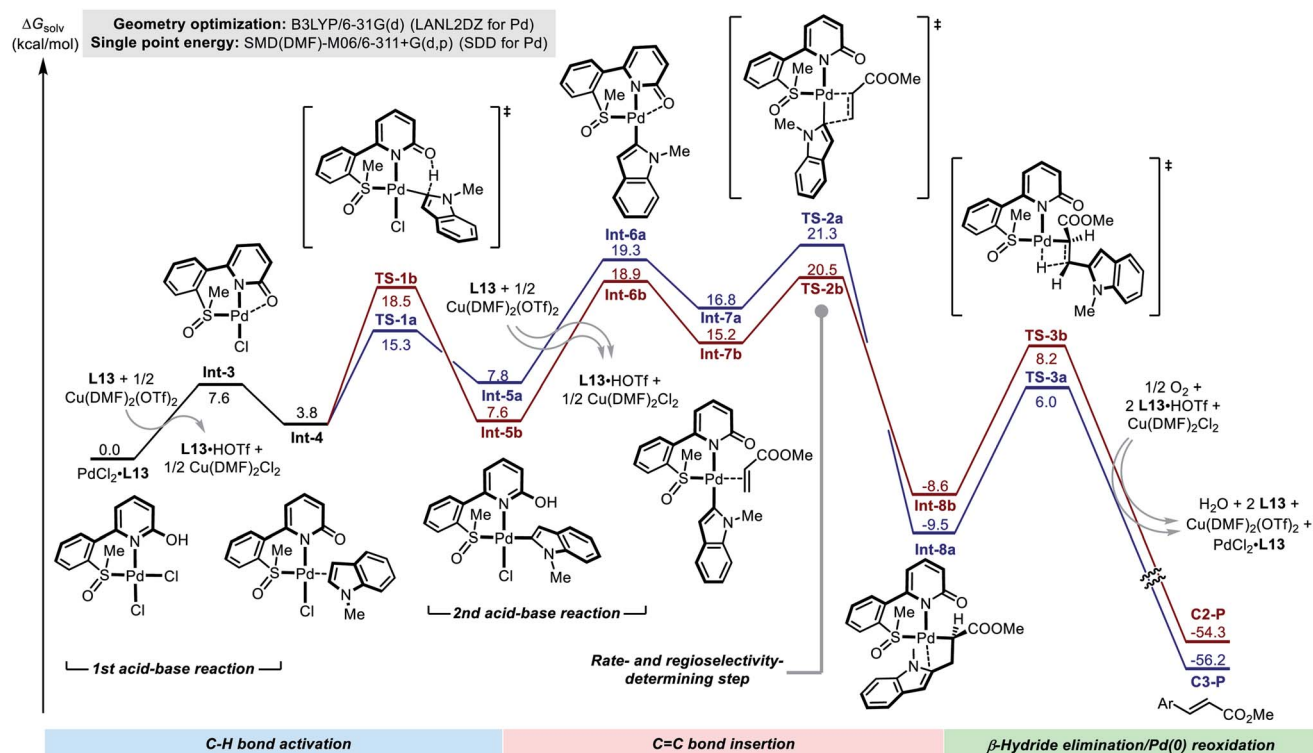


Fig. 2 The potential energy surface of the C–H alkenylation reaction of indole **1a**. Both C2- (red) and C3-alkenylation (blue) pathways are included, but only the intermediates and transition states in the C2-alkenylation pathway are shown for clarity.

facilitated the formation of **Int-3** from the initial PdCl<sub>2</sub>-SOHP complex. In **Int-3**, the SOHP ligand adopts a  $\kappa^3$ -S,N,O coordination mode, which brings about additional ring strain. The following substrate coordination releases this ring strain, affording complex **Int-4**.

**Int-4** is the bifurcating point of the potential energy surface, from which two C–H activation transition states (TSs) evolve and lead to the C3- and C2-alkenylation pathways, respectively. In both C3- and C2-palladation transition states **TS-1a** and **TS-1b**, the 2-hydroxypyridine moiety in the SOHP ligand acts as an internal base to abstract a proton from the indole C–H bond. This CMD mechanism greatly facilitated the C–H palladation on both C3- and C2-sites of indole, as compared with the corresponding palladation pathways in the ligand-free system (Scheme 2b). As revealed by DFT calculation, the C3-palladation ( $\Delta G^\ddagger = 15.3$  kcal mol<sup>−1</sup>) is still favored over C2-palladation ( $\Delta G^\ddagger = 18.5$  kcal mol<sup>−1</sup>), which indicates that the palladation step remains C3-selective, as the experimental studies have indicated (Scheme 5b).

The C–H palladation steps lead to the formation of C3- and C2-Pd indole species **Int-5a** and **Int-5b**. Afterwards, another HCl elimination process has to occur to generate **Int-6a** and **Int-6b**, which allow for acrylate coordination and alkene insertion. These acid–base reactions were also found to be endergonic ( $\Delta G > 10$  kcal mol<sup>−1</sup> for both pathways), even if the assistance of the base and the Cu(II) salt was considered. The alkene coordination occurs between these indolylpalladium species and the acrylate substrate to form **Int-7a** and **Int-7b**, and then migratory

insertion of the C–Pd bond to the C=C bond takes place via **TS-2a** and **TS-2b**. Notably, similar to the “ligand-free” alkenylation reaction (Scheme 2), the insertion step in the ligand-promoted reaction also exhibits a C2-selectivity. In the C2-alkenylation pathway, the insertion step has the highest activation barrier, but the activation energy barrier of the C–H palladation step is close (**TS1b** vs. **TS2b**), which is in agreement with the conclusions drawn from the experimental study. The  $\beta$ -hydride elimination steps are facile in both pathways (via **TS-3a** and **TS-3b**) and do not affect the rate or the regioselectivity.

The DFT calculation supported that the observed C2-alkenylation selectivity in the ligand-promoted reaction was a combined result of the quasi-reversible C–H activation and the regioselectivity-determining alkene insertion, which significantly differs from the original reaction without the SOHP ligand (Fig. 2 vs. Fig. S12<sup>†</sup>). This ligand-enabled switch of the regioselectivity-control mode confirmed our design concept. Computations also revealed that the Cu(II) salt employed in the Pd(II)/SOHP reaction system is not only a redox catalyst, but also plays an important role in promoting the reaction by assisting the elimination of HCl from the key Pd(II) species.

## 2.4 Scope of the ligand-enabled regioselective oxidative Heck reactions

The optimal SOHP ligand enabled the regioselective synthesis of C2-alkenylated indole derivatives, while the established method utilizing DMSO as the ligand led to C3-alkenylation of indoles. The present method enriched the toolbox for





regioselective functionalization of indoles under aerobic conditions. We performed the indole alkenylation reactions employing a variety of indole derivatives and electron deficient olefins under both conditions to explore the substrate scope.

**2,3-Unsubstituted indoles as substrates.** The indole derivatives with both C2- and C3-positions unsubstituted are ideal substrates to showcase the ligand-enabled regioselectivity control (Table 2). It was found that, indoles with different electronic substituents were suitable substrates for both methods. Under C2-alkenylation conditions, C2-products were

Table 2 Substrate scope of the oxidative alkenylation reactions of indole<sup>a</sup>

C2-alkenylation conditions		C3-alkenylation conditions	
Entry	C2-alkenylation conditions	C3-alkenylation conditions	
1	<b>3b<sup>b</sup></b> 58% yield	<b>3a</b> 76% yield	
2	<b>6b<sup>c</sup></b> 44% yield	<b>6a</b> 28% yield	
3	<b>7a + 7b<sup>c</sup></b> (C3/C2 = 12:1)	<b>7a</b> No reaction	
4	<b>8b<sup>c</sup></b> 55% yield	<b>8a</b> 71% yield	
5	<b>9b<sup>b,d</sup></b> 75% yield	<b>9a<sup>e</sup></b> 85% yield	
6	<b>10b</b> 60% yield	<b>10a</b> 86% yield	
7	<b>11b<sup>b,d</sup></b> 75% yield	<b>11a</b> 63% yield	
8	<b>12b<sup>b,d</sup></b> 84% yield	<b>12a</b> 55% yield	
9	<b>13b<sup>c</sup></b> 40% yield	<b>13a</b> 26% yield	
10	<b>14b<sup>b,d</sup></b> 39% yield	<b>14a</b> 16% yield	
11	<b>15b<sup>b,d</sup></b> 82% yield	<b>15a</b> No reaction	
12	<b>16b<sup>c</sup></b> 54% yield	<b>16a</b> 77% yield	
13	<b>17b<sup>c</sup></b> 54% yield	<b>17a</b> 75% yield	
14	<b>18b<sup>b</sup></b> 51% yield	<b>18a</b> 62% yield	
15	<b>19b<sup>c</sup></b> 50% yield	<b>19a</b> 53% yield	
16	<b>20b<sup>b</sup></b> 73% yield	<b>20a</b> 43% yield	
17	<b>21b<sup>c</sup></b> 22% yield	<b>21a</b> 41% yield	
18	<b>22b<sup>b</sup></b> 41% yield	<b>22a</b> 21% yield	

<sup>a</sup> For C2-alkenylation reactions, 2 equiv. of **1** and 1 equiv. of **2** were used; for C3-alkenylation reactions, 1 equiv. of **1** and 2 equiv. of **2** were used. Yields of isolated products were reported (for C2-alkenylation reactions, only the C2-products were isolated). <sup>b</sup> Reaction was performed at 50 °C. <sup>c</sup> 5 mol% PdCl<sub>2</sub>(CH<sub>3</sub>CN)<sub>2</sub> and 10 mol% Cu(OTf)<sub>2</sub> was used instead of 10 mol% PdCl<sub>2</sub>(CH<sub>3</sub>CN)<sub>2</sub> and 50 mol% Cu<sub>2</sub>(OH)<sub>2</sub>CO<sub>3</sub>. <sup>d</sup> 1 equiv. of **1** and 1.3 equiv. of **2** were used. <sup>e</sup> 10 mol% PdCl<sub>2</sub>(CH<sub>3</sub>CN)<sub>2</sub> was used.



produced predominately and C3-products were generated in minor amounts (except in entry 3); under C3-alkenylation conditions, C3-products were produced exclusively. Both *N*-methyl and free NH-indoles were compatible with both conditions, albeit the reactions of NH-indoles were generally inferior due to undesired oxidation of the substrate (entries 2, 9, and 10). Indoles bearing an electron-withdrawing *N*-substituent underwent alkenylation smoothly under the C2-alkenylation conditions, but were unreactive under the traditional C3-alkenylation conditions (entries 3 and 11), highlighting the remarkable promotive effect of the ligand on C–H activation. It is notable that, under the ligand-promoted alkenylation conditions, *N*-methoxycarbonylindole exhibited C2-selectivity (entry 11), while *N*-tosylindole still preferred C3-product formation (entry 3). Other electronic substituents on the C4–7 positions of indole, including halogen (entries 4–6 and 9), carboxylic ester (entry 7), cyano (entries 8 and 10), and methoxy groups (entry 11), were well tolerated under both conditions.

Other electron-deficient olefins, such as methyl, ethyl, cyclopropyl, and benzyl acrylates, acrylonitrile, and diethyl vinylphosphonate, could be employed as the alkenylation reagent in the reactions to afford the C2- or C3-alkenylation products under regioselective alkenylation conditions (entries 13–18). Notably, for the substrates tested, no trace of the C2-product was observed under the traditional C3-alkenylation conditions, and C2-alkenylation could only be enabled by using the Pd(II)/SOHP system, which emphasized the key role of the designed ligand for C–H activation at the C2-position.

The limitation of the present C2-alkenylation reaction was that the olefin substrate should be electron-deficient and mono-substituted. Disubstituted olefins, such as crotonates and  $\alpha$ -methyl acrylates, exhibited rather low reactivity and could not afford the alkenylation products in a reasonable yield. This might be caused by the high activation barrier of the alkene insertion step.

**3-Substituted indole derivatives as substrates.** From a synthetic point of view, the C2-alkenylation of C3-substituted indole substrates, such as tryptophan or tryptophol derivatives, is also highly useful. We found that, for substrates **1l** and **1m**, although the C3-position of indole is blocked, C2-alkenylation does not occur facily under the standard C3-alkenylation conditions due to the difficulty in C2-palladation.

Alternatively, utilizing the present Pd(II)/SOHP catalytic system, C2-alkenylation products **23** and **24** (obtained as a mixture of **24a** and **24b** due to partial desilylation of the silyl ether) were produced in good yields (Scheme 9). This feature might be useful in the functionalization of complex indole derivatives through C2-alkenylation.

### 3. Conclusion

In this work, we studied a new mode of regiocontrol in a transition-metal-catalyzed C–H functionalization reaction, which features a ligand-enabled switch of the regioselectivity-determining step. This mode has been demonstrated by the Pd(II)-catalyzed ligand-controlled C3/C2-selective aerobic oxidative Heck reaction of indole. A new type of ancillary ligand, sulfoxide-2-hydroxypyridine (SOHP), was developed based on a mechanistic understanding, which functioned as a key control factor in rendering the C2-selectivity of the reaction. This reaction represents a nice yet rare example of ligand-controlled regioselectivity in the direct C–H functionalization of heteroarenes.

The mode of ligand-directed regioselectivity control in this reaction has been clearly elucidated through a detailed mechanistic study. It was found that the C–H activation and the C=C insertion are two key steps in this oxidative Heck reaction, and under the traditional reaction conditions the C–H activation step with a C3-preference is rate- and regioselectivity-determining. The SOHP ligand facilitates C–H palladation by promoting proton abstraction *via* a CMD mechanism. As a result, the activation barriers of the C–H palladation step at both C3- and C2-sites are significantly decreased, rendering a quasi-reversible C–H activation step and a regioselectivity-determining C=C insertion step. The reaction exhibits the regioselectivity determined by the insertion step, which is C2-selective. The present reaction system perfectly exemplified the ligand-enabled switch of regioselectivity-determining step as an efficient mode of regiocontrol.

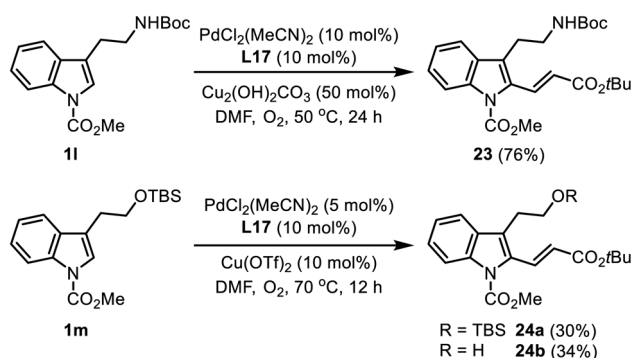
The mechanistic information acquired in this work shed some light on the regioselectivity control in related reaction systems. It reminds chemists that for many C–H activation reactions, the regio-preferences of both the C–H metalation and the following functionalization steps should be considered with equal attention. In case there is a discrepancy, a rational ligand design that allows for a switch of regioselectivity-determining step between these two processes may open an avenue to a new ligand-controlled regioselective reaction. We hope that this mode of regiocontrol is extendable to more substrate types, and it could inspire the design of more regiocontrolled C–H functionalization reactions.

### Conflicts of interest

There are no conflicts to declare.

### Acknowledgements

The National Natural Science Foundation of China (Grant No. 21822304) is acknowledged for financial support. The



Scheme 9 C2-alkenylation of tryptamine and tryptophol derivatives.



technology platform of CBMS and the Tsinghua Xuetao Talents Program are acknowledged for providing instrumentation and computational resources.

## References

- For reviews, see: (a) J.-Q. Yu and Z. Shi, *C–H Activation*, Springer, 2010, vol. 292; (b) T. W. Lyons and M. S. Sanford, *Chem. Rev.*, 2010, **110**, 1147–1169; (c) L. McMurray, F. O'Hara and M. J. Gaunt, *Chem. Soc. Rev.*, 2011, **40**, 1885–1898; (d) N. Kuhl, M. N. Hopkinson, J. Wencel-Delord and F. Glorius, *Angew. Chem., Int. Ed.*, 2012, **51**, 10236–10254; (e) S. R. Neufeldt and M. S. Sanford, *Acc. Chem. Res.*, 2012, **45**, 936–946; (f) P. H. Dixneuf and H. Doucet, *C–H Bond Activation and Catalytic Functionalization I*, Springer, 2016; (g) T. Gensch, M. N. Hopkinson, F. Glorius and J. Wencel-Delord, *Chem. Soc. Rev.*, 2016, **45**, 2900–2936; (h) J. Yamaguchi and K. Itami, *Bull. Chem. Soc. Jpn.*, 2017, **90**, 367–383; (i) D. Wang, A. B. Weinstein, P. B. White and S. S. Stahl, *Chem. Rev.*, 2018, **118**, 2636–2679; (j) P. Gandeepan, T. Muller, D. Zell, G. Cera, S. Warratz and L. Ackermann, *Chem. Rev.*, 2019, **119**, 2192–2452.
- (a) M. Zhang, Y. Zhang, X. Jie, H. Zhao, G. Li and W. Su, *Org. Chem. Front.*, 2014, **1**, 843–895; (b) Z. Chen, B. Wang, J. Zhang, W. Yu, Z. Liu and Y. Zhang, *Org. Chem. Front.*, 2015, **2**, 1107–1295; (c) J. Maes and B. U. W. Maes, *Adv. Heterocycl. Chem.*, 2016, **120**, 137–194; (d) G. Pototschnig, N. Maulide and M. Schnürch, *Chem.–Eur. J.*, 2017, **23**, 9206–9232; (e) W. Ma, P. Gandeepan, J. Li and L. Ackermann, *Org. Chem. Front.*, 2017, **4**, 1435–1467; (f) C. Sambaglio, D. Schönbauer, R. Blicke, T. Dao-Huy, G. Pototschnig, P. Schaaf, T. Wiesinger, M. F. Zia, J. Wencel-Delord, T. Besset, B. U. W. Maes and M. Schnürch, *Chem. Soc. Rev.*, 2018, **47**, 6603–6743.
- For selected examples of template-directed regioselective C–H functionalizations, see: (a) J. Spencer, B. Z. Chowdhry, A. I. Mallet, R. P. Rathnam, T. Adatia, A. Bashall and F. Rominger, *Tetrahedron*, 2008, **64**, 6082–6089; (b) D. Leow, G. Li, T.-S. Mei and J.-Q. Yu, *Nature*, 2012, **486**, 518–522; (c) L. Wan, N. Dastbaravardeh, G. Li and J.-Q. Yu, *J. Am. Chem. Soc.*, 2013, **135**, 18056–18059; (d) G. Yang, P. Lindovska, D. Zhu, J. Kim, P. Wang, R.-Y. Tang, M. Movassaghi and J.-Q. Yu, *J. Am. Chem. Soc.*, 2014, **136**, 10807–10813; (e) S. Bag, T. Patra, A. Modak, A. Deb, S. Maity, U. Dutta, A. Dey, R. Kancherla, A. Maji, A. Hazra, M. Bera and D. Maiti, *J. Am. Chem. Soc.*, 2015, **137**, 11888–11891; (f) Z. Jin, L. Chu, Y.-Q. Chen and J.-Q. Yu, *Org. Lett.*, 2018, **20**, 425–428.
- For selected examples of intrinsic regiocontrol in the C–H functionalization of heterocycles, see: (a) H. Choi, M. Min, Q. Peng, D. Kang, R. S. Paton and S. Hong, *Chem. Sci.*, 2016, **7**, 3900–3909; (b) A. M. Prendergast and G. P. McGlacken, *Eur. J. Org. Chem.*, 2018, 6068–6082 and references therein.
- For selected reviews, see: (a) K. M. Engle and J.-Q. Yu, *J. Org. Chem.*, 2013, **78**, 8927–8955; (b) L. Ping, D. S. Chung, J. Bouffard and S. G. Lee, *Chem. Soc. Rev.*, 2017, **46**, 4299–4328; (c) M. T. Mihai, G. R. Genov and R. J. Phipps, *Chem. Soc. Rev.*, 2018, **47**, 149–171; (d) V. K. Tiwari and M. Kapur, *Org. Biomol. Chem.*, 2019, **17**, 1007–1026.
- For selected examples of the ligand-promoted palladium-catalyzed C–H functionalization reactions, see: (a) A. N. Campbell, E. B. Meyer and S. S. Stahl, *Chem. Commun.*, 2011, **47**, 10257–10259; (b) A. Vasseur, C. Laugel, D. Harakat, J. Muzart and J. Le Bras, *Eur. J. Org. Chem.*, 2015, 944–948; (c) B. F. Shi, N. Maugel, Y. H. Zhang and J. Q. Yu, *Angew. Chem., Int. Ed.*, 2008, **47**, 4882–4886; (d) D. H. Wang, K. M. Engle, B. F. Shi and J. Q. Yu, *Science*, 2010, **327**, 315–319; (e) L. Chu, K. J. Xiao and J. Q. Yu, *Science*, 2014, **346**, 451–455; (f) P. X. Shen, L. Hu, Q. Shao, K. Hong and J. Q. Yu, *J. Am. Chem. Soc.*, 2018, **140**, 6545–6549; (g) Q.-F. Wu, X.-B. Wang, P.-X. Shen and J.-Q. Yu, *ACS Catal.*, 2018, **8**, 2577–2581; (h) S. Ma and S. Yu, *Tetrahedron Lett.*, 2004, **45**, 8419–8422; (i) Y. Izawa and S. S. Stahl, *Adv. Synth. Catal.*, 2010, **352**, 3223–3229; (j) J. A. Schiffrer and M. Oestreich, *Eur. J. Org. Chem.*, 2011, 1148–1154; (k) M. H. Emmert, A. K. Cook, Y. J. Xie and M. S. Sanford, *Angew. Chem., Int. Ed.*, 2011, **50**, 9409–9412; (l) J. He, S. Li, Y. Deng, H. Fu, B. N. Laforteza, J. E. Spangler, A. Homs and J. Q. Yu, *Science*, 2014, **343**, 1216–1220; (m) W.-L. Jia and M. Á. Fernández-Ibáñez, *Eur. J. Org. Chem.*, 2018, 6088–6091; (n) H. Shi, P. Wang, S. Suzuki, M. E. Farmer and J. Q. Yu, *J. Am. Chem. Soc.*, 2016, **138**, 14876–14879; (o) P. Wang, P. Verma, G. Xia, J. Shi, J. X. Qiao, S. Tao, P. T. W. Cheng, M. A. Poss, M. E. Farmer, K. S. Yeung and J. Q. Yu, *Nature*, 2017, **551**, 489–493; (p) R. Y. Zhu, Z. Q. Li, H. S. Park, C. H. Senanayake and J. Q. Yu, *J. Am. Chem. Soc.*, 2018, **140**, 3564–3568; (q) M. S. Chen and M. C. White, *J. Am. Chem. Soc.*, 2004, **126**, 1346–1347; (r) T. J. Osberger and M. C. White, *J. Am. Chem. Soc.*, 2014, **136**, 11176–11181; (s) K. Yamaguchi, H. Kondo, J. Yamaguchi and K. Itami, *Chem. Sci.*, 2013, **4**, 3753–3757; (t) H. Kondo, F. Yu, J. Yamaguchi, G. Liu and K. Itami, *Org. Lett.*, 2014, **16**, 4212–4215; (u) W. Liu, S. Z. Ali, S. E. Ammann and M. C. White, *J. Am. Chem. Soc.*, 2018, **140**, 10658–10662; (v) R. Ma and M. C. White, *J. Am. Chem. Soc.*, 2018, **140**, 3202–3205; (w) W. H. Henderson, C. T. Check, N. Proust and J. P. Stambuli, *Org. Lett.*, 2010, **12**, 824–827; (x) C. C. Le, K. Kunchithapatham, W. H. Henderson, C. T. Check and J. P. Stambuli, *Chem.–Eur. J.*, 2013, **19**, 11153–11157; (y) B. J. Gorsline, L. Wang, P. Ren and B. P. Carrow, *J. Am. Chem. Soc.*, 2017, **139**, 9605–9614.
- For selected examples of ligands used in other transition-metal catalyzed C–H functionalization reactions, see: (a) R. Bisht and B. Chattopadhyay, *J. Am. Chem. Soc.*, 2016, **138**, 84–87; (b) S. Okumura, S. Tang, T. Saito, K. Semba, S. Sakaki and Y. Nakao, *J. Am. Chem. Soc.*, 2016, **138**, 14699–14704; (c) Y. Nakao, K. S. Kanyiva and T. Hiyama, *J. Am. Chem. Soc.*, 2008, **130**, 2448–2449; (d) Y. Nakao, Y. Yamada, N. Kashihara and T. Hiyama, *J. Am. Chem. Soc.*, 2010, **132**, 13666–13668; (e) Y. Kuninobu, H. Ida, M. Nishi and M. Kanai, *Nat. Chem.*, 2015, **7**, 712–717; (f) H. J. Davis and R. J. Phipps, *Chem. Sci.*, 2017, **8**, 864–877; (g)





- H. J. Davis, M. T. Mihai and R. J. Phipps, *J. Am. Chem. Soc.*, 2016, **138**, 12759–12762; (h) J. M. Alderson, A. M. Phelps, R. J. Scamp, N. S. Dolan and J. M. Schomaker, *J. Am. Chem. Soc.*, 2014, **136**, 16720–16723.
- 8 (a) S. Yanagisawa, K. Ueda, H. Sekizawa and K. Itami, *J. Am. Chem. Soc.*, 2009, **131**, 14622–14623; (b) K. Ueda, S. Yanagisawa, J. Yamaguchi and K. Itami, *Angew. Chem., Int. Ed.*, 2010, **49**, 8946–8949.
- 9 Regiocontrol by switch of the regioselectivity-determining step was rather rare in transition-metal catalysis (not limited to C–H functionalization reactions). For examples, see: (a) I. A. Sanhueza, A. M. Wagner, M. S. Sanford and F. Schoenebeck, *Chem. Sci.*, 2013, **4**, 2767–2775; (b) E. P. Jackson and J. Montgomery, *J. Am. Chem. Soc.*, 2015, **137**, 958–963.
- 10 For selected reviews on C–H functionalization of indole, see: (a) M. Bandini and A. Eichholzer, *Angew. Chem., Int. Ed.*, 2009, **48**, 9608–9644; (b) E. M. Beck and M. J. Gaunt, *Top. Curr. Chem.*, 2010, **292**, 85–121; (c) L. Joucla and L. Djakovitch, *Adv. Synth. Catal.*, 2009, **351**, 673–714; (d) A. H. Sandtorv, *Adv. Synth. Catal.*, 2015, **357**, 2403–2435; (e) J. A. Leitch, Y. Bhonoah and C. G. Frost, *ACS Catal.*, 2017, **7**, 5618–5627; (f) M. Petrini, *Chem.–Eur. J.*, 2017, **23**, 16115–16151; (g) J.-B. Chen and Y.-X. Jia, *Org. Biomol. Chem.*, 2017, **15**, 3550–3567; (h) J. Kalepu, P. Gandeepan, L. Ackermann and L. T. Pilarski, *Chem. Sci.*, 2018, **9**, 4203–4216; (i) T. A. Shah, P. B. De, S. Pradhan and T. Punniyamurthy, *Chem. Commun.*, 2019, **55**, 572–587.
- 11 For selected recent examples on Pd-catalyzed functionalization of indole, see: (a) K.-Y. Jia, J.-B. Yu, Z.-J. Jiang and W.-K. Su, *J. Org. Chem.*, 2016, **81**, 6049–6055; (b) Y. Yang, X. Qiu, Y. Zhao, Y. Mu and Z. Shi, *J. Am. Chem. Soc.*, 2016, **138**, 495–498; (c) Y. Yang, P. Gao, Y. Zhao and Z. Shi, *Angew. Chem., Int. Ed.*, 2017, **56**, 3966–3971; (d) A. J. Borah and Z. Shi, *Chem. Commun.*, 2017, **53**, 3945–3948; (e) M. N. Godoi, F. de Azambuja, P. D. G. Martinez, N. H. Morgon, V. G. Santos, T. Regiani, D. Lesage, H. Dossmann, R. B. Cole, M. N. Eberlin and C. R. D. Correia, *Eur. J. Org. Chem.*, 2017, 1794–1803; (f) T. Hanakawa, K. Isa, S. Isobe, Y. Hoshino, B. Zhou and M. Kawatsura, *J. Org. Chem.*, 2017, **82**, 2281–2287; (g) S. Zhao, W. Ma, M. Yasir, X. Zhou, J. Cheng and C. Jiang, *ChemistrySelect*, 2018, **3**, 13319–13322; (h) O. Moncea, D. Poinot, A. A. Fokin, P. R. Schreiner and J.-C. Hierso, *ChemCatChem*, 2018, **10**, 2915–2922; (i) S. Fang, G. Jiang, M. Li, Z. Liu, H. Jiang and W. Wu, *Chem. Commun.*, 2019, **55**, 13769–13772; (j) N. Thrimurtulu, A. Dey, A. Singh, K. Pal, D. Maiti and C. M. R. Volla, *Adv. Synth. Catal.*, 2019, **361**, 1441–1446; (k) S. Guo, Z. Fang, B. Zhou, J. Hua, Z. Dai, Z. Yang, C. Liu, W. He and K. Guo, *Org. Chem. Front.*, 2019, **6**, 627–631; (l) J. Zhang, M. Wu, J. Fan, Q. Xua and M. Xie, *Chem. Commun.*, 2019, **55**, 8102–8105; (m) P.-G. Li, Y. Yang, S. Zhu, H.-X. Li and L.-H. Zou, *Eur. J. Org. Chem.*, 2019, 73–76.
- 12 B. Karimi, H. Behzadnia, D. Elhamifar, P. F. Akhavan, F. K. Esfahani and A. Zamani, *Synthesis*, 2010, 1399–1427.
- 13 For selected examples on the oxidative Heck reaction of indole, see: (a) P. S. Baran and E. J. Corey, *J. Am. Chem. Soc.*, 2002, **124**, 7904–7905; (b) G. Abbiati, E. M. Beccalli, G. Broggini and C. Zoni, *J. Org. Chem.*, 2003, **68**, 7625–7628; (c) E. M. Ferreira and B. M. Stoltz, *J. Am. Chem. Soc.*, 2003, **125**, 9578–9579; (d) S. Ma and S. Yu, *Tetrahedron Lett.*, 2004, **45**, 8419–8422; (e) N. P. Grimster, C. Gauntlett, C. R. Godfrey and M. J. Gaunt, *Angew. Chem., Int. Ed.*, 2005, **44**, 3125–3129; (f) L. Djakovitch and P. Rouge, *Catal. Today*, 2009, **140**, 90–99; (g) Q. Huang, Q. Song, J. Cai, X. Zhang and S. Lin, *Adv. Synth. Catal.*, 2013, **355**, 1512–1516; (h) H. P. Gemoets, V. Hessel and T. Noel, *Org. Lett.*, 2014, **16**, 5800–5803.
- 14 For selected examples of regioselectivity switchable C–H arylation reactions of indole, see: (a) B. S. Lane, M. A. Brown and D. Sames, *J. Am. Chem. Soc.*, 2005, **127**, 8050–8057; (b) D. R. Stuart, E. Villemure and K. Fagnou, *J. Am. Chem. Soc.*, 2007, **129**, 12072–12073; (c) R. J. Phipps, N. P. Grimster and M. J. Gaunt, *J. Am. Chem. Soc.*, 2008, **130**(26), 8172–8174.
- 15 For selected examples of C2-alkenylation of indoles by the directing group strategy, see: (a) E. Capito, J. M. Brown and A. Ricci, *Chem. Commun.*, 2005, 1854–1856; (b) A. Maehara, H. Tsurugi, T. Satoh and M. Miura, *Org. Lett.*, 2008, **10**, 1159–1162; (c) A. Garcia-Rubia, R. Gomez Arrayas and J. C. Carretero, *Angew. Chem., Int. Ed.*, 2009, **48**, 6511–6515; (d) A. Garcia-Rubia, B. Urones, R. Gomez Arrayas and J. C. Carretero, *Chem.–Eur. J.*, 2010, **16**, 9676–9685; (e) L. Wang, W. Guo, X. X. Zhang, X. D. Xia and W. J. Xiao, *Org. Lett.*, 2012, **14**, 740–743; (f) Z.-L. Yan, W.-L. Chen, Y.-R. Gao, S. Mao, Y.-L. Zhang and Y.-Q. Wang, *Adv. Synth. Catal.*, 2014, **356**, 1085–1092.
- 16 For an example of solvent-controlled regioselective C–H alkenylation on pyrroles, see: Y. Su, H. Zhou, J. Chen, J. Xu, X. Wu, A. Lin and H. Yao, *Org. Lett.*, 2014, **16**, 4884–4887.
- 17 The calculations were performed using the Gaussian 09 software package. For computational details and the full citation of Gaussian 09, see the ESI.†
- 18 S. Zhang, Z. Chen, S. Qin, C. Lou, A. M. Senan, R. Z. Liao and G. Yin, *Org. Biomol. Chem.*, 2016, **14**, 4146–4157.
- 19 For selected reviews on 2-hydroxypyridine in ligand design, see: (a) J. M. Rawson and R. E. P. Winpenny, *Coord. Chem. Rev.*, 1995, **139**, 313–374; (b) J. R. Khusnutdinova and D. Milstein, *Angew. Chem., Int. Ed.*, 2015, **54**, 12236–12273; (c) C. M. Moore, E. W. Dahl and N. K. Szymczak, *Curr. Opin. Chem. Biol.*, 2015, **25**, 9–17; (d) M. W. Drover, J. A. Love and L. L. Schafer, *Chem. Soc. Rev.*, 2017, **46**, 2913–2940; (e) T. Higashi, S. Kusumoto and K. Nozaki, *Chem. Rev.*, 2019, **119**, 10393–10402; (f) K. Fujita, *Bull. Chem. Soc. Jpn.*, 2019, **92**, 344–351.
- 20 P. Wang, M. E. Farmer and J. Q. Yu, *Angew. Chem., Int. Ed.*, 2017, **56**, 5125–5129.
- 21 V. Salamanca, A. Toledo and A. C. Albeniz, *J. Am. Chem. Soc.*, 2018, **140**, 17851–17856.
- 22 For selected examples and reviews, see: (a) B. A. Steinhoff, S. R. Fix and S. S. Stahl, *J. Am. Chem. Soc.*, 2002, **124**, 766–



- 767; (b) W. Zierkiewicz and T. Privalov, *Organometallics*, 2005, **24**, 6019–6028; (c) B. A. Steinhoff and S. S. Stahl, *J. Am. Chem. Soc.*, 2006, **128**, 4348–4355; (d) T. N. Diao, P. White, I. Guzei and S. S. Stahl, *Inorg. Chem.*, 2012, **51**, 11898–11909; (e) G. Sipos, E. E. Drinkel and R. Dorta, *Chem. Soc. Rev.*, 2015, **44**, 3834–3860.
- 23 (a) A. H. Jackson and P. P. Lynch, *J. Chem. Soc., Perkin Trans. 2*, 1987, 1483–1488; (b) X. Guo, S. Pan, J. Liu and Z. Li, *J. Org. Chem.*, 2009, **74**, 8848–8851.
- 24 We have found that the addition of a base (2,6-di-*tert*-butylpyridine) could accelerate the C2-deuteration reaction, which is consistent with the proposed reaction mechanism that deprotonation from the PdCl<sub>2</sub>·L17 complex is important for the reaction. Thus we hypothesized that the faster deuteration rate in the actual catalytic reaction was due to the existence of metal oxide species (generated from the aerobic re-oxidation of Pd(0)) as the base. For more details, see the ESI.†
- 25 L. Wang and B. P. Carrow, *ACS Catal.*, 2019, **9**, 6821–6836.

